Asociación Argentina
de Mecánica Computacional

Mecánica Computacional Vol XXIX, págs. 1627-1647 (artículo completo)
Eduardo Dvorkin, Marcela Goldschmit, Mario Storti (Eds.)
Buenos Aires, Argentina, 15-18 Noviembre 2010

FLUID-STRUCTURE INTERACTION USING AN ARBITRARY LAGRANGIAN-EULERIAN FLUID SOLVER COUPLED TO A POSITIONAL LAGRANGIAN SHELL SOLVER

Rodolfo A. K. Sanches and Humberto B. Coda

Departamento de Engenharia de Estruturas, Escola de Engenharia de São Carlos, Universidade de São Paulo, São Carlos, SP, Brasil, raks@sc.usp.br, http://www.set.eesc.usp.br

Keywords: Positional fem, Non-linear geometric shell, Fluid-structure interaction, Arbitrary Lagrangian-Eulerian formulation.

Abstract. This work consists of the development of a partitioned 3D computational code for non linear geometrical fluid-structure interaction analysis using the Finite Element Method. The fluid solver is explicit and its time integration is based on characteristics, which introduces automatically stabilizing terms on stream direction. The Navier-Stokes equations are written in the arbitrary Lagrangian-Eulerian (ALE) description, in order to accept moving boundaries and coupling with Lagrangian shell elements. The structure is modeled using a positional FEM formulation to deal with geometrical nonlinear dynamics of shells using a methodology based on the minimum potential energy theorem written regarding nodal positions and generalized unconstrained vectors, not displacements and rotations. These characteristics avoid the use of large rotation approximations.The coupling between the two different meshes is done by mapping the fluid boundary nodes local positions over the shell elements and *vice versa*, avoiding the need of matching fluid and shell nodes. The fluid mesh is adapted using one simple approach based shell positions and velocities. The efficiency and robustness of the proposed approach is demonstrated by examples.

1 INTRODUCTION

The fluid structure interaction problem is present in various engineering activities, as civil buildings, mechanical devices, aeronautics, ocean structures and biomechanics. As simple examples one may mention the wind effect over buildings, airplane or stayed bridges flutter, and even the arterial inflation or deflation due to blood circulation.

The complexity and high number of calculus operations involved on fluid-structure interaction analysis, leads to the search for computational techniques to help solving adequately such problems. The fact that structures are being projected more slender and slight on recent times, and so, much more susceptible to fluid-structure interaction problems, has also made increase the need for computational tools even more precises and efficients dedicated to this area.

The objective of this paper is to present an efficient and versatile numerical model for fluid-shell interaction. This paper develops firstly an algorithm for fluid dynamics with moving boundaries, then the geometrical non-linear shell solver is presented and finally a partitioned non-matching nodes coupling algorithm is developed.

Traditionally the mathematical model for physics problems is done in a Eulerian or Lagrangian description. The Lagrangian description expresses the continuum medium movement in terms of the initial configuration and time, being very efficient for problems where finite displacements are the main variables, such as in solid mechanics. By other hand, the Eulerian description is deffined in terms of final configuration and time, being well used for problems where the variables are velocities instead of displacements, such as for fluid mechanics (Valiappan, 1981).

A robust way to couple these two mediums is to solve the solid based on a Lagrangian description and the fluid based on an Arbitrary Lagrangian-Eulerian (ALE) description (Donea et al., 1982), which is also employed by many works on last decade (Teixeira and Awruch, 2005; Bathe and Zhang, 2004; Garelli et al., 2010).

In many fluid-structure interaction problems it is important to carry a geometric non-linear analysis due to large displacements or due to coupled membrane and bending effects. This work employs a novel geometric non-linear formulation for shell analysis based on positions which was introduced by Greco and Coda (2004) and is being satisfactorily developed and extended to more complex problems (Maciel and Coda, 2005; Coda and Paccola, 2009; Coda, 2009; Coda and Paccola, 2010)

The fluid solver is explicit and its time integration is based on characteristics, which introduces automatically stabilizing terms on stream direction stabilizing the spurious variations introduced by the employment of the standard Galerkin procedure (Zienkiewicz and Taylor, 2000).

The algorithm is tested by comparison of numerical examples proposed with numerical and experimental results from the literature.

2 FEM FOR FLUID MECHANICS WITH MOVING BOUNDARIES

2.1 Arbitrary Lagrangian-Eulerian description of the fluid mechanics governing equations

The Eulerian description of fluid dynamics governing equations (Navier-Stokes) is well known, leading to the equations:

$$\frac{\partial \rho}{\partial t} = -\frac{\partial (\rho u_i)}{\partial x_i}, \tag{1}$$

which is the mass conservation equation,

$$\frac{\partial(\rho u_i)}{\partial t} = -\frac{\partial(u_j \rho u_i)}{\partial x_j} + \frac{\partial \tau_{ij}}{\partial x_j} - \frac{\partial p}{\partial x_i} + \rho g_i, \tag{2}$$

which is the momentum equation, and

$$\frac{\partial(\rho E)}{\partial t} = -\frac{\partial}{\partial x_j}(u_j \rho E) + \frac{\partial}{\partial x_i}\left(k\frac{\partial T}{\partial x_i}\right) - \frac{\partial}{\partial x_j}(u_j p) + \frac{\partial}{\partial x_j}(\tau_{ij} u_j) + \rho g_i u_i, \tag{3}$$

which is the energy equation. In these equations ρ is the specific mass, u_i is the i velocity component, with i being the Cartesian axe 1, 2 or 3 (x, y or z), p is the pressure, τ_{ij} are the deviatoric stress tensor (i, j) components, g_i is the i direction field forces constant, E is the specific energy, T is the temperature ans k is the thermal conductivity.

The Arbitrary Lagrangian-Eulerian (ALE) description is obtained by introducing a reference $R(t)$ domain with arbitrary movement when deriving the governing equations. It may be considered as a mapping from the initial configuration $C(t_0)$ to the final configuration $C(t)$, written with respect to the moving reference domain (Donea et al., 1982) (see Fig. 1). Considering the fem mesh as the domain $R(t)$, this approach leads to a method where the mesh is allowed to move in an arbitrary way. For fluid structure-interaction analysis this movement should be compatible to the structure movement (Sanches and Coda, 2008b,a).

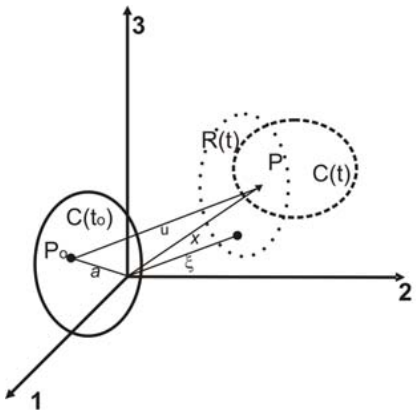

Figure 1: Adopted kinematics for ALE description

The Jacobian J which represent the transformation from the the reference domain $R(t)$ to the material domain $C(t_0)$ is given by:

$$J = \det\left(\frac{\partial \xi_i}{\partial a_j}\right) \text{ with } i \text{ and } j = 1, 2 \text{ or } 3, \tag{4}$$

where ξ_i and a_j are the position vectors components regarding respectively to $R(t)$ and $C(T_0)$.

Deriving Eq. (4) regarding to time results

$$\frac{\partial J}{\partial t} = J\nabla \cdot \overrightarrow{w}, \tag{5}$$

where $\overrightarrow{w}$ is the reference domain ($R(t)$) velocity.

Considering a physical property expressed at reference configuration as $f(\xi_i, t)$ and equal to $F(a_i, t)$ at the initial configuration, it is possible to write:

$$\frac{\partial F(a_i,t)}{\partial t} = \left.\frac{\partial f(\xi_i,t)}{\partial t}\right|_{\xi} + \frac{\partial f(\xi_i,t)}{\partial \xi_i}\left(\frac{\partial \xi_i}{\partial t}\right). \tag{6}$$

Based on the derivative rules applied to $\nabla(fw)$ and based also on Eq. (5), Eq. (6) may be re-written as:

$$\frac{\partial (JF)}{\partial t} = J\left[\frac{\partial f}{\partial t} + \nabla\cdot(fw)\right]. \tag{7}$$

Substituting $f = \rho$ on Eq. (7) and taking in account the mass conservation equation ((1)) one may write using index notation:

$$\frac{\partial(\rho J)}{\partial t} = J\frac{\partial\left(\rho(w_i - u_i)\right)}{\partial x_j}, \tag{8}$$

or, from Eq.(5):

$$\frac{\partial \rho}{\partial t} + \frac{\partial(\rho u_i)}{\partial x_i} = w_i\frac{\partial \rho}{\partial x_i}, \tag{9}$$

which is the final form for the mass conservation equation on ALE description.

Following the same procedure for (1) and (2), the ALE formulation for momentum and energy equation are obtained as:

$$\frac{\partial(\rho u_i)}{\partial t} + \frac{\partial(u_j\rho u_i)}{\partial x_j} - \frac{\partial \tau_{ij}}{\partial x_j} + \frac{\partial p}{\partial x_i} - \rho g_i = w_j\frac{\partial(\rho u_i)}{\partial x_j} \tag{10}$$

and

$$\frac{\partial(\rho E)}{\partial t} + \frac{\partial(u_j\rho E)}{\partial x_j} - \frac{\partial}{\partial x_i}\left(k\frac{\partial T}{\partial x_i}\right) + \frac{\partial(u_j p)}{\partial x_j} - \frac{\partial(\tau_{ij}u_j)}{\partial x_j} - \rho g_i u_i = w_i\frac{\partial(\rho E)}{\partial x_i}. \tag{11}$$

It is important to observe that if the velocity w is null, the formulation rely on the Eulerian description, while if $w = u$ the formulation rely on the Lagrangian description (Donea et al., 1982).

2.2 Time integration along characteristics

Characteristics are the curves that indicate the spatial positions by where a given property ϕ is transported (Fortuna, 2000) (see Fig 2).

If there is no diffusion, the time variation of ϕ over a characteristic of coordinates x' is by definition null:

$$\frac{d\phi}{dt}(x', t) = 0. \tag{12}$$

For the Navier-Stokes equations we can write:

$$\frac{\partial \phi(x', t)}{\partial t} - Q(x') = 0, \tag{13}$$

where $Q(x')$ contains all the non convective terms.

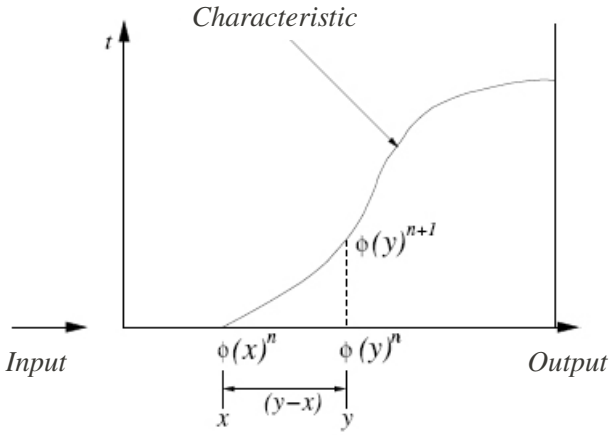

Figure 2: Characteristics for non-linear convection

We assume the following approximation for Eq. (13) (Zienkiewicz and Taylor, 2000):

$$\frac{\phi(y)_{n+1} - \phi(x)_n}{\Delta t} \approx \theta(Q(y)_{n+1}) + (1-\theta)(Q(x)_n), \tag{14}$$

where x and y means respectively the characteristic positions at $t = n$ and $t = n+1$, θ is a constant with value 0 for explicit solution and may be chosen larger than zero 0 and smaller than 1 for semi-implicit or implicit solution.

The product $u\phi$ and the term $Q(x)$ may be approximated by Taylor resulting the following expressions:

$$u\phi(x)_n = u\phi(y)_n - (y-x)\frac{\partial(u\phi(y))_n}{\partial x} + \frac{(y-x)^2}{2}\frac{\partial^2(u\phi(y)_n)}{\partial x^2} + O(\Delta t^3), \tag{15}$$

$$Q(x)_n = Q(y)_n - (y-x)\frac{\partial Q(y)_n}{\partial x} + O(\Delta t^2). \tag{16}$$

Dividing Eq. (15) by u and substituting on Eq. (14), then substituting $Q(x)_n$ by Eq. (16) and assuming $\theta = 0$ (explicit form), results:

$$\frac{1}{\Delta t}\left(\phi(y)_{n+1} - \phi(y)_n + \frac{(y-x)}{u}\frac{\partial(u\phi(y))_n}{\partial x} - \frac{(y-x)^2}{2u}\frac{\partial^2(u\phi(y)_n)}{\partial x^2}\right) = Q(y)_n - (y-x)\frac{\partial Q(y)_n}{\partial x} + O(\Delta t^2)\,. \tag{17}$$

Assuming $\Delta t = (y-x)/u$ on Eq. (17) and reorganizing, we have:

$$\phi(y)_{n+1} = \phi(y)_n - \Delta t\left(\frac{\partial(u\phi(y))_n}{\partial x} - Q(y)_n\right) + \frac{(\Delta t)^2}{2}u\frac{\partial}{\partial x}\left(\frac{\partial(u\phi(y)_n)}{\partial x} - Q(y)_n\right) + O(\Delta t^2). \tag{18}$$

One important point about this procedure is that the high order terms of Eq. (18), obtained due to time integration along characteristics, introduce dissipation on stream lines direction, which as shown by Zienkiewicz and Taylor (2000) are equivalent to the SUPG schemes when the time interval tends to the critical time interval, and gets smaller effects as the time interval get smaller.

2.2.1 Navier-Stokes equations discretization

From the same procedure that produced Eq. (18), applied to Eq. (10), one may write:

$$\begin{aligned}\Delta(\rho u_i)_{n+1} = \Delta t \left(-\frac{\partial(u_j \rho u_i)}{\partial x_j} + w_j \frac{\partial(\rho u_i)}{\partial x_j} + \frac{\partial \tau_{ij}}{\partial x_j} - \frac{\partial p}{\partial x_i} + \rho g_i \right)_n + \\ \frac{\Delta t^2}{2} \left(u_k \frac{\partial}{\partial x_k} \left(\frac{\partial(u_j \rho u_i)}{\partial x_j} - w_j \frac{\partial(\rho u_i)}{\partial x_j} - \frac{\partial \tau_{ij}}{\partial x_j} + \frac{\partial p}{\partial x_i} - \rho g_i \right) \right)_n ,\end{aligned} \tag{19}$$

where all the right hand side terms are known on instant $t = n$.

Based on the Eulerian mass conservation equation, Zienkiewicz and Taylor (2000) suggest the following expression for explicit solution:

$$\Delta \rho_{n+1} = -\Delta t \frac{\partial \left(\rho u_i\right)_{n+\theta}}{\partial x_i} = -\Delta t \left(\frac{\partial}{\partial x_i} \left(\rho u_i\right)_n + \theta \frac{\partial \left(\Delta \left(\rho u_i\right)\right)_{n+1}}{\partial x_i} \right), \tag{20}$$

where θ is a arbitrary constant with value between 0.5 and 1.

For the ALE case, we keep the same scheme adding the terms due to mesh movement obtained by the expansion of the full mass conserving equation, resulting on the following expression:

$$\begin{aligned}\Delta \rho_{n+1} = -\Delta t \left(\frac{\partial}{\partial x_i} \left(\rho u_i\right)_n + \theta \frac{\partial \left(\Delta \left(\rho u_i\right)\right)_{n+1}}{\partial x_i} + w_i \frac{\partial \rho}{\partial x_i} \right) + \\ \frac{\Delta t^2}{2} \left(u_k \frac{\partial}{\partial x_k} \left(-w_i \frac{\partial \rho}{\partial x_i} \right) \right)_n .\end{aligned} \tag{21}$$

Finally, applying to Eq. (11) the same procedure that produced (19), we have:

$$\begin{aligned}\Delta(\rho E)_{n+1} = \Delta t \left(-\frac{\partial(u_i \rho E)}{\partial x_i} + w_i \frac{\partial(\rho E)}{\partial x_i} \right)_n + \\ \Delta t \left(\frac{\partial}{\partial x_i} \left(k \frac{\partial T}{\partial x_i} \right) - \frac{\partial(u_i p)}{\partial x_i} + \frac{\partial(\tau_{ij} u_j)}{\partial x_i} - \rho g_i u_i \right) + \\ \frac{\Delta t^2}{2} u_k \frac{\partial}{\partial x_k} \left(\frac{\partial(u_i \rho E)}{\partial x_i} - w_i \frac{\partial(\rho E)}{\partial x_i} \right) + \\ \frac{\Delta t^2}{2} u_k \frac{\partial}{\partial x_k} \left(-\frac{\partial}{\partial x_i} \left(k \frac{\partial T}{\partial x_i} \right) + \frac{\partial(u_i p)}{\partial x_i} - \frac{\partial(\tau_{ij} u_j)}{\partial x_i} + \rho g_i u_i \right)_n .\end{aligned} \tag{22}$$

2.3 FEM discretization

Applying the Galerkin method to Eq. (19), (21) and (22), in order to obtain the spatial discretization, making use of divergence theorem and neglecting the boundary high order terms,

we get the following expressions:

$$\begin{aligned}\int_\Omega \mathbf{N}\Delta(\rho u_i)d\Omega = \Delta t \int_\Omega \mathbf{N}\left(-\frac{\partial(u_j\rho u_i)}{\partial x_j} + w_j\frac{\partial(\rho u_i)}{\partial x_j} + \rho g_i\right)d\Omega \\ -\Delta t\left(\int_\Omega \frac{\partial \mathbf{N}}{\partial x_j}(\tau_{ij}-\delta_{ij}p)d\Omega + \int_\Gamma \mathbf{N}(\tau_{ij}n_j - pn_i)d\Gamma\right), \\ -\frac{\Delta t^2}{2}\int_\Omega \frac{\partial(\mathbf{N}u_k)}{\partial x_k}\left(\frac{\partial}{\partial x_j}(u_j\rho u_i) - w_j\frac{\partial}{\partial x_j}(\rho u_i) - \frac{\partial \tau_{ij}}{\partial x_j} + \frac{\partial p}{\partial x_i} - \rho g_i\right)d\Omega\end{aligned} \tag{23}$$

$$\begin{aligned}\int_\Omega \mathbf{N}\Delta\rho d\Omega = \Delta t\int_\Omega\left(\frac{\partial \mathbf{N}}{\partial x_i}(\rho u_i + \theta\Delta(\rho u_i)) - \frac{\partial(\mathbf{N}w_i)}{\partial x_i}\rho\right)d\Omega + \\ \frac{\Delta t^2}{2}\int_\Omega\left(\frac{\partial(\mathbf{N}u_k)}{\partial x_k}w_i\frac{\partial\rho}{\partial x_i}\right)d\Omega - \\ \Delta t\int_\Gamma \mathbf{N}\left(\rho u_i + \theta\Delta(\rho u_i) - \rho w_i + \frac{\Delta t}{2}w_i\frac{\partial\rho}{\partial x_i}\right)n_i d\Gamma,\end{aligned} \tag{24}$$

and

$$\begin{aligned}\int_\Omega \mathbf{N}\Delta(\rho E)d\Omega = \Delta t\int_\Omega \mathbf{N}\left(-\frac{\partial\left(u_i(\rho E+p)\right)}{\partial x_i}d\Omega + w_i\frac{\partial(\rho E)}{\partial x_i}\right)d\Omega - \\ \Delta t\int_\Omega\frac{\partial\mathbf{N}}{\partial x_i}\left(\tau_{ij}u_j + k\frac{\partial T}{\partial x_i}\right)d\Omega + \\ \frac{\Delta t^2}{2}\int_\Omega\frac{\partial\left(u_j\mathbf{N}\right)}{\partial x_j}\left(\frac{\partial(-u_i(\rho E+p))}{\partial x_i} + w_i\frac{\partial(\rho E)}{\partial x_i}\right)d\Omega + \\ \Delta t\int_\Gamma\phi\left(\tau_{ij}u_j + k\frac{\partial T}{\partial x_i}\right)n_i d\Gamma,\end{aligned} \tag{25}$$

where $\mathbf{N}$ is the shape functions vector.

Writing in a matrix form we have:

$$\mathbf{M}\overline{\rho\mathbf{u}}_i = \Delta t\mathbf{f}_\mathbf{u}, \tag{26}$$

$$\mathbf{M}\overline{\mathbf{\Delta}\rho} = \Delta t\mathbf{f}_\rho \tag{27}$$

and

$$\mathbf{M}\Delta\overline{\rho\mathbf{E}} = \Delta t\mathbf{f}_\mathbf{e} \tag{28}$$

where $\mathbf{f_u}$, $\mathbf{f}_\rho$ and $\mathbf{f_e}$ are the right hand side vectors and $\mathbf{M}$ is the mass matrix given by:

$$\mathbf{M} = \int_\Omega \mathbf{N}^T\mathbf{N}d\Omega, \tag{29}$$

The mass matrix $\mathbf{M}$ may be easily lumped, which is highly desirable for explicit methods. However the use of consistent mass matrix can prevent spurious variations when Δt is small, as presented by Zienkiewicz and Taylor (2000).

Therefore, we employ the interactive approach to solve the systems based on mass balance given by:

$$(\mathbf{\Delta}\phi)_l = (\mathbf{\Delta}\phi)_{l-1} + \mathbf{M_L}^{-1}\left[\mathbf{B} - \mathbf{M}\,(\mathbf{\Delta}\phi)_{l-1}\right], \tag{30}$$

where $\mathbf{\Delta}\phi$ is the unknowns vector, l is the interaction step, $\mathbf{M_L}$ is the lumped matrix, $\mathbf{M}$ is the consistent mass matrix and $\mathbf{B}$ is the right hand side vector. This procedure converges very fast to the consistent solution for $\mathbf{\Delta}\phi$.

Solving Eqs. (26),(27),and (26), all the variables can be computed on instant $t = n+1$ based on the thermodynamic equations.

2.4 Shock capturing

We still need to choose a shock capturing technique, as the standard Galerkin method is unable to deal with strong discontinuities, such as shock waves.

Therefore we add an artificial dissipative term based on the pressure second derivative, given by the following expression:

$$f_{\mu_a} = \Delta t \mu_a \frac{\partial}{\partial x_i}\left(\frac{\partial \phi}{\partial x_i}\right), \tag{31}$$

where ϕ is the variable to be smoothed and μ_a is the artificial viscosity given by:

$$\mu_a = q_{dif} h^3 \frac{(|\mathrm{u}| + c)}{p_{med}} \left|\frac{\partial}{\partial x_i}\left(\frac{\partial p}{\partial x_i}\right)\right|_e, \tag{32}$$

where u is the velocity absolute value, p_{med} is the pressure average over the element, q_{dif} is an user coefficient taken between 0 and 2, c is the sound speed and h is the element size.

3 POSITIONAL FEM FOR GEOMETRICAL NONLINEAR DYNAMICS OF SHELLS

The methodology employed is based on the minimum potential energy theorem written regarding nodal positions and generalized unconstrained vectors instead of displacements and rotations. This characteristic avoid the use of large rotation approximations The shell formulation is total Lagrangian and, due to its unconstrained vector mapping, it presents constant mass matrix and therefore it is possible to apply the Newmak β integrator as a momentum conserving algorithm.

3.1 Strain measure and specific strain energy potential

We employ the Green strain tensor to derive the proposed formulation. The Green strain tensor is derived directly from the gradient of the configuration change function as depicted on Fig. 3, represented by letter A, given as follows:

$$A_{ij} = \frac{\partial \chi_i}{\partial X_j} \tag{33}$$

where χ is the configuration change function, and X represents variation regarding initial position.

Following Ogden (1984), the Green strain tensor can be written as:

$$E_{ij} = \frac{1}{2}\left[A_{ki}A_{kj} - \delta_{ij}\right] = \frac{1}{2}\left[C_{ij} - \delta_{ij}\right] \tag{34}$$

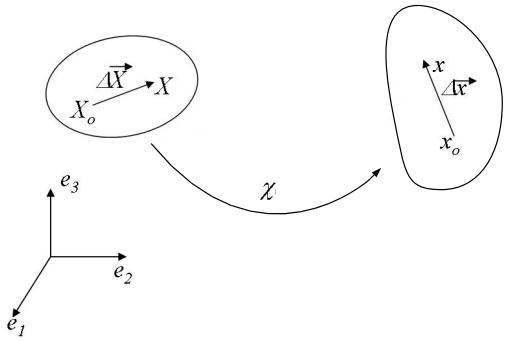

Figure 3: Change of configuration

The variables C_{ij} and δ_{ij} are the right Cauchy-Green stretch tensor and the Kroenecker delta, respectively. The following quadratic strain energy per unit of initial volume is adopted,

$$u_e = \frac{1}{2} E_{ij} C_{ijkl} E_{kl} \tag{35}$$

resulting into a linear elastic constitutive law relating second Piola-Kirchhoff stress and Green strain, usually called Saint-Venant–Kirchhoff elastic law, i.e.:

$$S_{ij} = \frac{\partial u_e}{\partial E_{ij}} = C_{ijkl} E_{kl} \tag{36}$$

The elastic tensor is given by

$$C_{ijkl} = \frac{2G\nu}{1-2\nu} \delta_{ij}\delta_{kl} + G(\delta_{ik}\delta_{jl} + \delta_{il}\delta_{jk}) \tag{37}$$

Where G is the shear modulus.

The true stress (Cauchy stress) is achieved directly from the Second Piolla-Kirchhoff stress following simple expressions given by Ogden (1984), for instance.

3.2 Positional shell formulation

Shell structures consists on solids with one dimension much larger than the others.Therefore Coda and Paccola (2009) develop the shell formulation based on the middle surface configuration change as depicted on Fig. (4).

The fictitious configuration change functions f^{m0} and f^{m1}, from an auxiliary non-dimensional space respectively to the initial and final configurations may be written as follows:

$$f_i^{m0} = X_i^m(\xi_1, \xi_2, X_{ji}) = N_j(\xi_1, \xi_2) X_{ji}^m \tag{38}$$

e

$$f_i^{m1} = x_i^m(\xi_1, \xi_2, x_{ji}) = N_j(\xi_1, \xi_2) x_{ji}^m, \tag{39}$$

For any point out of the middle surface, its position at initial and final configuration may be written as:

$$X_i = X_i^m + g_i^0, \tag{40}$$

and

$$x_i = x_i^m + g_i^1, \tag{41}$$

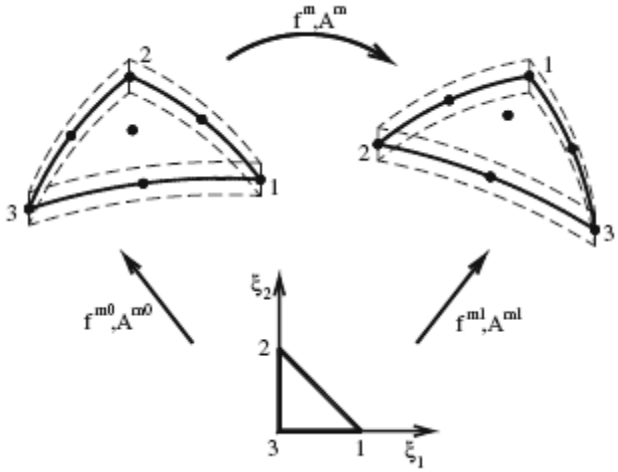

Figure 4: Middle surface mapping

where the g^0 and g^1 are called generalized position vectors for the initial and final configurations.

Considering a linear strain rate along the thickness, the vectors g^0 and g^1 may be written as (Coda and Paccola, 2009):

$$g_i^0 = \frac{h_0}{2}\xi_3 N_j(\xi_1,\xi_2)e_{ij}^0 \tag{42}$$

and

$$g_i^1 = \frac{h_0}{2}\left[\xi_3 + a(\xi_1,\xi_2)\xi_3^2\right]\ N_j(\xi_1,\xi_2)\,\bar{G}_{ij} \tag{43}$$

where $\bar{G}_{ij}$ are the nodal values (unknowns) for the generalized vector at node *j* at final configuration, h^0 and h are respectively the initial thickness and final thickness, e_i^0 and e_i^1 and the i components for unitary vectors $\overrightarrow{e^0}$ and $\overrightarrow{e^1}$, normal to the midle surface at initial and final configuration and a is the strain rate along thickness.(see Fig. 5).

Finally, the real middle surface configuration change from initial to final configurations is represented by:

$$\overrightarrow{f}^m = \overrightarrow{f}^m\left(\overrightarrow{X}^m\right) = \left(\overrightarrow{f}^{m1}\right) \circ \left(\overrightarrow{f}^{m0}\right)^{-1} \tag{44}$$

The gradient $\mathbf{A}^m$ of the configuration change function may be expressed by:

$$\mathbf{A}^m = Grad\left(\overrightarrow{f}^m\right) = \frac{\partial \overrightarrow{f}^m}{\partial \overrightarrow{X}^m} = \left(\mathbf{A}^{m1}\right)\left(\mathbf{A}^{m0}\right)^{-1}. \tag{45}$$

Using the shape functions, one may write $\mathbf{A}^{m0}$ and $\mathbf{A}^{m1}$ as:

$$A_{ij}^{m0} = f_{i,j}^{m0} = N_{k,j}(\xi_1,\xi_2,\xi_3)X_{ki}, \tag{46}$$

and

$$A_{ij}^{m1} = f_{i,j}^{m1} = N_{k,j}(\xi_1,\xi_2,\xi_3)x_{ki}, \tag{47}$$

where the indexes ,*j* indicate derivatives on direction *j*.

After evaluating the gradient $\mathbf{A}$, the Green strain tensor and the specific strain energy may be obtained from Eqs. (34) and (35).

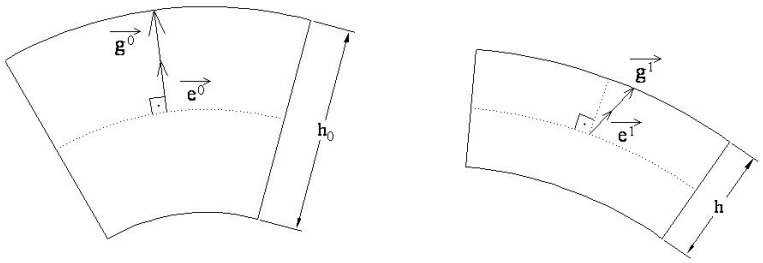

Initial configuration *Final configuration*

Figure 5: Generalized vectors

3.2.1 The adopted shell element

The finite element adopted in for this paper is an isoparametric triangular element with 10 nodes (cubic shape functions). Each node has 7 nodal parameters: 3 position vector components x_i with $i = 1, 2$ or 3, 3 components of the generalized position vector $\bar{G}_i$ with $i = 1, 2$ or 3 and the strain ratio along thickness a.

3.3 Time integration

The time integrator employed is the Newmark β, which is summarized as:

$$x_{S+1} = x_S + \Delta t \dot{x}_S + \Delta t^2 \left[\left(\frac{1}{2} - \beta \right) \ddot{x}_S + \beta \ddot{x}_{S+1} \right] \tag{48}$$

and

$$\dot{x}_{S+1} = \dot{x}_S + \Delta t \left(1 - \gamma\right) \ddot{x}_S + \gamma \Delta t \ddot{x}_{S+1}. \tag{49}$$

Coda and Paccola (2009) proved that for a positional total Lagrangian description, the Newmark β with $\gamma = 1/2$ presents momentum and energy conservative properties for most of shell dynamics problems.

3.4 Newton-Raphson procedure

From preceding developments, one may write the equilibrium equation as the minimization of the energy functional as:

$$\frac{\partial \mathbf{U_e}}{\partial x} - \mathbf{F} + \mathbf{M}\ddot{\mathbf{x}} + \mathbf{C}\dot{\mathbf{x}} = 0, \tag{50}$$

where $\mathbf{F}$ is the external forces vector, C is the dissipative matrix and $\mathbf{M}$ is the mass matrix.

At instant t_{S+1}, the equilibrium is expressed by the following equation:

$$\left.\frac{\partial \Pi}{\partial x}\right|_{S+1} = \left.\frac{\partial \mathbf{U_e}}{\partial x}\right|_{S+1} - \mathbf{F_{S+1}} + \mathbf{M}\ddot{\mathbf{x}}_{\mathbf{S+1}} + \mathbf{C}\dot{\mathbf{x}}_{\mathbf{S+1}} = 0. \tag{51}$$

From Newmark β method, Eq. (48) and Eq. (49), the equation Eq. (51) becomes:

$$f\left(x_{S+1}\right) = \left.\frac{\partial \Pi}{\partial x}\right|_{S+1} = \left.\frac{\partial \mathbf{U_e}}{\partial x}\right|_{S+1} - \mathbf{F_{S+1}} + \frac{\mathbf{M}}{\beta \Delta t^2}\mathbf{x_{S+1}} - \mathbf{M Q_S} + \mathbf{C R_S} + \frac{\gamma \mathbf{C}}{\beta \Delta t}\mathbf{x_{S+1}} - \gamma \Delta t \mathbf{C Q_S} = 0, \tag{52}$$

where the vectors Q_s and R_s represent the dynamic contribution from the past and are expressed by:

$$\mathbf{Q_S} = \frac{\mathbf{x_S}}{\beta \Delta t^2} + \frac{\dot{\mathbf{x}}_\mathbf{S}}{\beta \Delta t} + \left(\frac{1}{2\beta} - 1\right)\ddot{\mathbf{x}}_\mathbf{S} \tag{53}$$

and

$$\mathbf{R_S} = \dot{\mathbf{x}}_\mathbf{S} + \Delta t\left(1 - \gamma\right)\ddot{\mathbf{x}}_\mathbf{S}. \tag{54}$$

The second energy functional variation is expressed by:

$$\left.\frac{\partial^2 \Pi}{\partial x^2}\right|_{S+1} = \nabla \mathbf{f}\left(\mathbf{x_{s+1}}\right) = \left.\frac{\partial^2 \mathbf{U_e}}{\partial \mathbf{x^2}}\right|_{S+1} + \frac{\mathbf{M}}{\beta \Delta t^2} + \frac{\gamma \mathbf{C}}{\beta \Delta t}. \tag{55}$$

An Taylor series first order approximation for the energy functional f gives:

$$0 = f(x) \cong f\left(x^0\right) + \nabla f\left(x^0\right)\Delta x. \tag{56}$$

The Newton-Raphson process for each time step is summarized on estimate a value x^0_{s+1} for the final position x_{s+1}, and apply the interactive process:

$$\nabla f\left(x^l_s\right)\Delta x = -f\left(x^l_s\right) \tag{57}$$

$$x^{l+1}_{S+1} = x^l + \Delta x, \tag{58}$$

where l is the interactions number. The interactions are interrupted when the admissible error prescribed is reached.

4 FLUID-STRUCTURE COUPLING PROCEDURE

We employ the partitioned coupling scheme, which allows to integrate fluid and solid by independent algorithms and then transfer the boundary condition from one media to the other. These scheme makes easy to change only the fluid dynamics solver or only the solid dynamics solver, allowing the evolution of the research.

5 FORCES AND VELOCITIES TRANSFERS

As fluid and shell mesh are different and generated in an independent process, during the pre-processing step, for each fluid node i, a closest point Ps_i at shell mesh domain (Ω_s) is identified and stored (see Fig. 5. Subsequently, the fluid mesh is adapted moving the node i to the exact position of Ps_i.

Finally, for each shell node k , a closest point Pf_k on the fluid boundary related to the structure (Γ_s) is identified and stored.

The Dirichlet boundary conditions for node i are obtained from the shell point Ps_i.

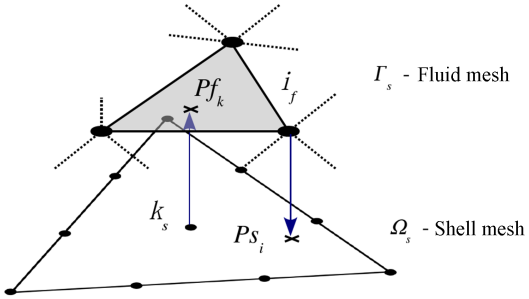

Figure 6: Transfer points

For viscous flow $\mathbf{u}_f(i) = \mathbf{u}_s(Ps_i)$ while for inviscid flow we adopt:

$$\mathbf{u}_f(i) = \mathbf{u}_f(i) + [(\mathbf{u}_s(i) - \mathbf{u}_f(i)) \cdot \mathbf{n}]\mathbf{n}. \tag{59}$$

where $\mathbf{u}_f$ is the fluid velocity vector, $\mathbf{u}_s$ is the shell velocity vector and $\mathbf{n}$ is the unity vector normal to Γ_s.

The Neumman boundary conditions for node k are obtained from fluid point Pf_k by the following expression:

$$q_{kj} = \left[-\tau_{jl} n_l - p n_l\right]_{Pf_k}, \tag{60}$$

where the indexes j and l represent Cartesian direction and n_l is the l component form the normal vector to Γ_s.

6 FLUID MESH DYNAMIC MOVING

The ALE formulation enables the arbitrary imposition of movement to the fluid mesh. A good mesh moving algorithm for fluid-structure interaction problems will adapt the fluid mesh to the solid movement with minimal of mesh distortion.

The Laplace equation would be a good choice for a mesh moving model, however it makes necessary to solve a new equation system. Therefore we adopted a technique similar to the one employed by Teixeira (2001). This technique consists on distribute the fluid mesh velocities based on the distance to the boundary according to:

$$w_i^k = \frac{\sum_{j=1}^{ne} a_{kj} u_i^j}{\sum_{j=1}^{ne} a_{kj} + \sum_{l=1}^{nf} b_{kl}}, \tag{61}$$

where *ne* is the shell nodes number, *nf* is the fixed boundary (Γ_f) nodes number, a_{kj} is the weight coefficient that takes in account the shell movement influence, and b_{kl} is the coefficient that takes in account the fixed boundary influence.

The coefficients a and b are given by:

$$a_{kj} = \frac{1}{d_{kj}^{e1}} \tag{62}$$

and

$$b_{kl} = \frac{1}{d_{kl}^{e2}}, \tag{63}$$

where d_{kj} is the distance between the node k and the node j located at the moving boundary, d_{kl} is the distance between the node k and the node l located at fixed fixed boundary, and $e1$

and *e2* are number chosen by the operator and enable to adjust the boundary influence over the mesh movement. A good choice for open flow problems is $e1 = e2 = 4$, however for closed flows with large displacements a smaller number may present better results.

7 COUPLING DYNAMIC PROCESS

As the shell solver is implicit and the fluid solver explicit, a coupling scheme which enable sub-cycles of time steps is desirable. Therefore we suggest the scheme depicted on Fig. 7.

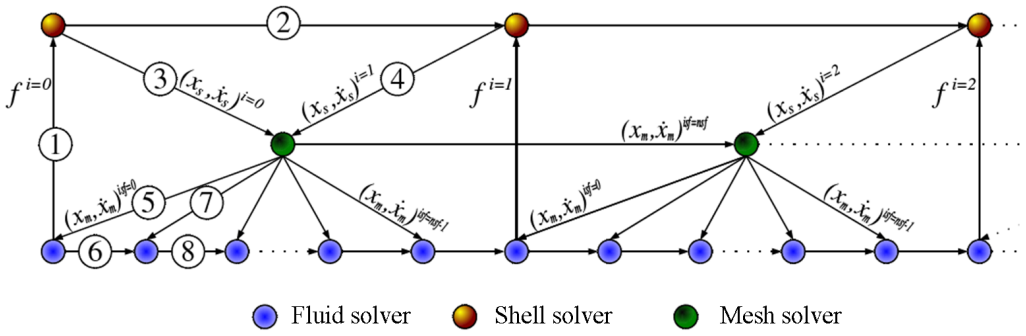

Figure 7: Coupling scheme

This scheme may be summarized as:

1. At a given instant $t_s = i$, the structure is solved with the loads imposed by the flow, with a time step Δt_s, resulting on final velocities and positions at instant $t_s = i + 1$.

2. The shell positions variation inside the time interval Δt_s is approximated by a cubic polynomial obtained based on $x_s(i)$ e $\dot{x}_s(i)$, $x_s(i+1)$ and $\dot{x}_s(i+1)$. From this polynomial the velocities and positions at each fluid time step $\Delta t_f = (\Delta t_s)/nsf$ are defined and the mesh movement is obtained from Eq. (61).

3. The fluid Dirichlet boundary conditions are obtained from the shell movement and the fluid is solved using time steps Δt_f until reaches the instant $t_f = i * nsf$, when fluid loads are imposed to the structure and the process restart.

8 NUMERICAL EXAMPLES

8.1 Panel Flutter

In this example the behavior of an initially flat panel clamped on both ends subjected to supersonic flow is analyzed. The flow is considered inviscid and the undisturbed flow has specific mass $\rho_\infty = 0.339$ kg/m^3 and pressure $p_\infty = 28$ KPa and sound speed $c = 340$ m/s, while the panel has: specific mass $\rho_s = 2710$ kg/m^3, Young's modulus $E = 77.28$ GPa and Poisson's ration $\nu = 0.33$, length 0.5 m, width 0.025 m and thickness 1.35 mm. The boundary conditions at $z = 0$ and $z = 0.025$m are those of symmetry regarding to the plane xy.

At the beginning of the analysis, the pressure on the inferior face of the panel is reduced from 0.1 %, introducing a disturbance to the panel. This condition is kept until 4 ms, when pressure on the inferior face is set again to p_∞.

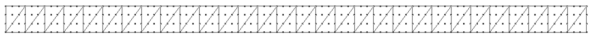

Figure 8: Panel mesh

The shell is modeled by 60 elements and 484 nodes (see Fig. 8), while the fluid is modeled by 58195 elements and 12566 nodes and the mesh geometry close to the panel is depicted on Fig. 11.

In order to compare with linear solutions from the literature, the membrane effect is eliminated by prescribing a free horizontal displacement at the end of the panel. This is expected to present results very close to the linear analysis for small displacements. The time steps adopted are $\Delta t_f = 10^{-7} s$ for fluid and $\Delta t_s = 10^{-6} s$ for shell. The vertical displacements at $x = 0.35$ m for $Mach$ number 1.90, 1.95, 2.00 and 2.05 are depicted on Fig. 9(a). From these results one may note that $Mach = 2.0$ appears critically dumped, what agrees with the linear aeroelastic solution using the piston theory (Teixeira and Awruch, 2005). The solution for $Mach = 2.00$ is compared with linear solutions obtained by other authors (see Fig. 9(b)) showing good agreement.

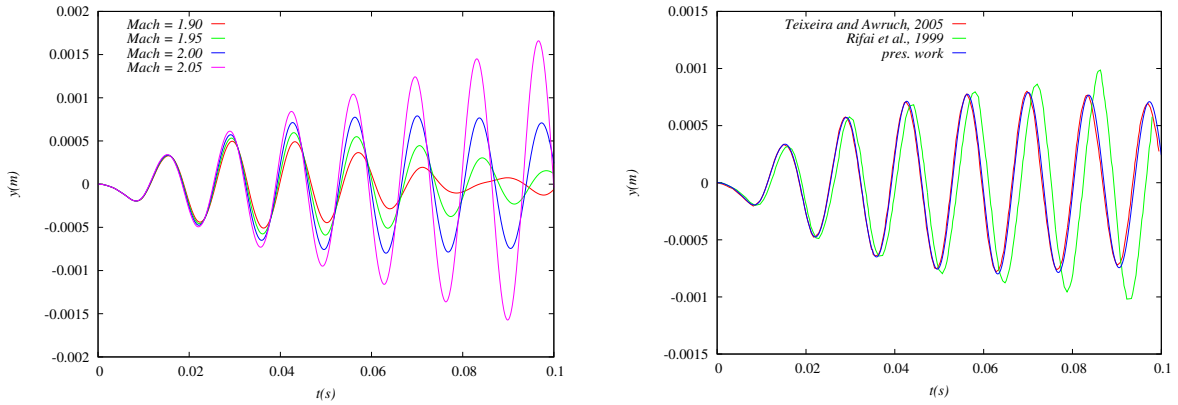

(a) Different $Mach$ numbers (b) $Mach = 2$ - different authors

Figure 9: Vertical displacement vs. time at $x = 0,35$

A non-linear analysis for the panel fully clamped on both ends for $Mach = 2.30$ is compared with the previous boundary conditions and with the results according to Teixeira and Awruch (2005) on Fig. 10(a) and compared with the non-linear solution obtained by Rifai et al. (1999) and with the solution considering larger Δt_s on Fig. 10(b). One may observe that for the non-linear analysis the membrane effect leads the structure to a non-dumped limit cycle instead an continuously increasing amplitude.

On Fig. 10(a) one may observe phase difference between the non-linear solution obtained by present work and by Teixeira and Awruch (2005) after 0.007 s. It is done to a non dominant mode coupled to the main mode which affected more the reference solution producing the phase alteration. This difference may be explained by the employment of completely different meshes, elements, formulations an time steps.

Observing Fig. 10(b) one may conclude that the reducing the structure time step the solution converges to one a bit different of the one presented by Rifai et al. (1999).

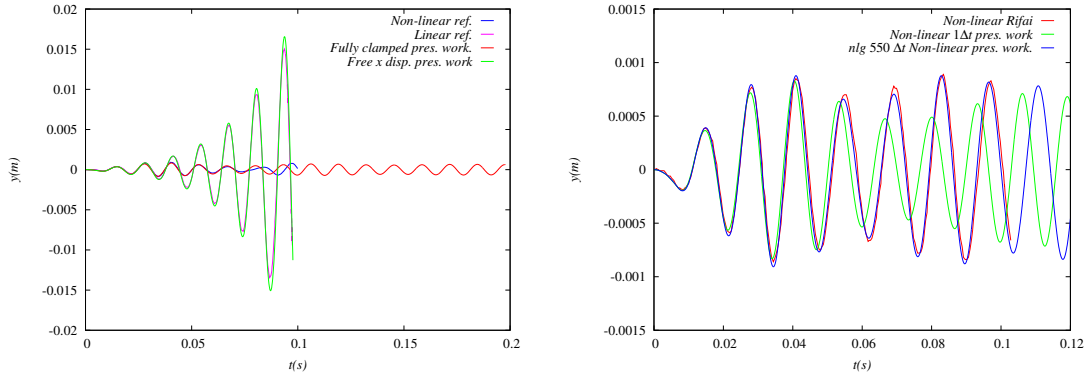

(a) Compared to Teixeira and Awruch (2005) (b) Compared to Rifai et al. (1999)

Figure 10: Vertical displacement vs. time at $x = 0,35$ for $Mach = 2.3$

Finally, Fig. 11 presents a snapshot of fluid pressure and shell deformation at times t = 0.074 s and t = 0.0805 s for $Mach = 2.30$ and free horizontal displacements at the end of panel.

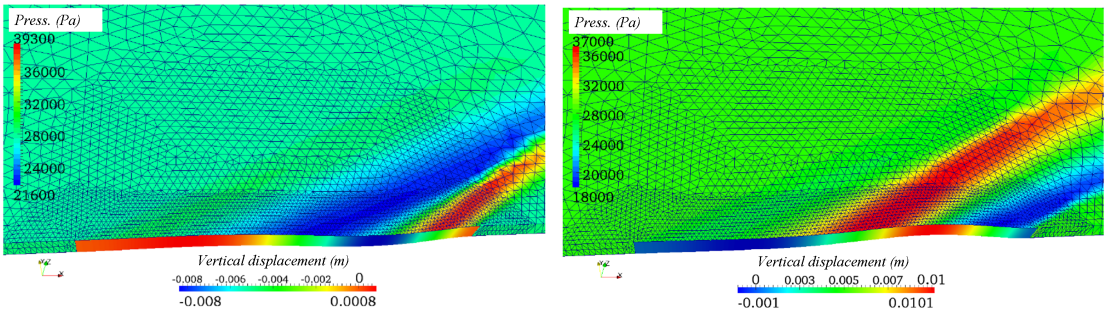

(a) t = 0.074 s (b) t = 0.0805 s

Figure 11: Pressure and displacements snapshots for $Mach = 2.3$

8.2 Vertical plate exposed to shock

This example compares an experimental case, performed by the IUSTI laboratory (Giordano et al., 2005) with the results computed by the proposed numerical model. Such experimental device describes a flexible panel protruding into a shock tube and submitted to a shock wave. A close-up view of the experimental set-up is given in Fig. 12. The panel is fixed in a base assumed infinitely rigid and the shock travels from left to right.

The coupled simulation is performed considering a linear elastic panel with a Young's Modulus $E = 220$ GPa and a density $\rho_s = 7600$ kg/m^3 with a length equal to 50 mm and 1 mm thickness. Considering the short duration of the experimental run, turbulence is neglected. The air is initially at standard atmosphere conditions ($p_\infty = 105$ kPa and $T_\infty = 293$K), and the shock wave is produced applying inlet boundary condition based on the Rankine–Hugoniot conditions for a $Mach$ number of shock wave $M_s = 1.2$.

As the problem is 2D, we discretized the domain with a thickness of 2.5 mm. The panel is divided into 40 elements and 244 nodes, while the fluid is divided into 72945 elements and 20617 nodes.

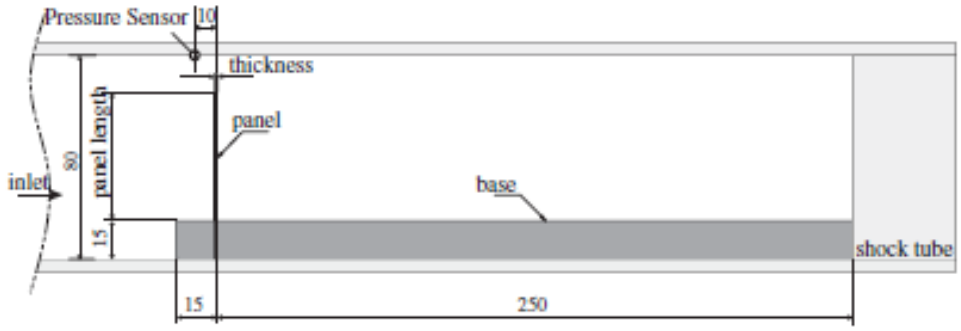

Figure 12: Problem geometry adapted from Giordano et al. (2005)

The flow field capture is qualitatively analysed on Fig. 13 by comparison of numerical Schlierens obtained by the magnitude of specific mass gradient with experimental experimental ombroscopic pictures extracted from Giordano et al. (2005) showing good agreement.

(a) t= 140 μs

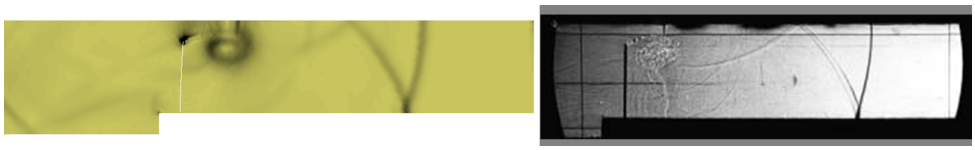

(b) t= 420 μs

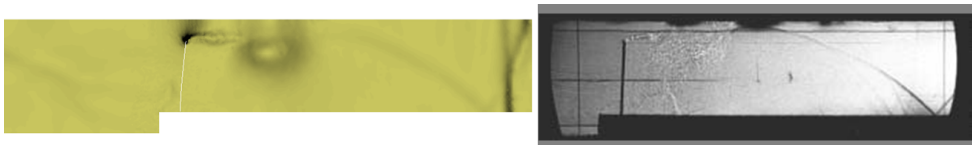

(c) t= 700 μs

(d) t= 980 μs

Figure 13: Numerical Schlieren vs. experimental pictures obtained by Giordano et al. (2005)

A pressure distribution and shell displacement snapshot at $t = 140\mu$ s is depicted on Fig. 14.

A quantitative evaluation is performed on Figs. 15 by comparing the horizontal displacement at the panel top with numerical results according to Giordano et al. (2005), and the pressure measured at the position indicated at Fig. 12 showing good agreement.

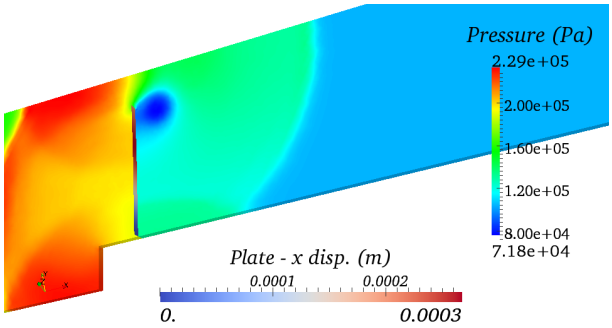

Figure 14: Pressure and horizontal displacements at t=140 μs

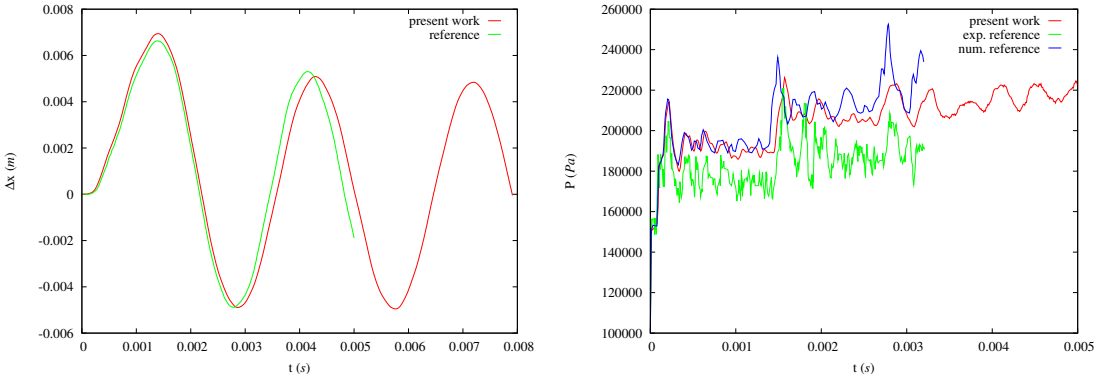

(a) Top horizontal displacements (b) Pressure at sensor position (Fig. 12)

Figure 15: Quantitative comparison to Giordano et al. (2005)

8.3 Explosion in a reactor containment

As a final example we present a simulation of a hypothetical gas explosion in a reactor-like containment with the same geometry used by Casadei and Halleux (1995). The problem geometry and meshes are depicted by Fig.16. The shell is discretized by 2323 nodes and 486 elements, and the fluid by 23585 nodes and 125470 elements. The lower basement of the container is very thick, therefore it is simply modeled by a rigid boundary in the present analysis. The container is supposed to be initially filled up with air at standard atmospheric conditions (represented by a perfect gas) at room. The shell properties are Young modulus $E = 21GPa$, Poisson ratio $\nu = .2$ and specific mass $\rho_s = 2500kg/m^3$. The fluid initially at rest has specific mass $\rho_f = 1.2kg/m^3$ specific heat ratio $\gamma = 1.4$, pressure $p = 10^5Pa$ and sound speed $c = 341.57m/s$.

An explosion with and the explosive are has initially $\rho_{exp} = 21.527kg/m^3$ and $p_{exp} = 69446Pa$ is assumed in the lower part of the container at the initial time of the studied transient ($t = 0$) is simulated by air at high pressure, initially occupying the lower part of the tank ($z < 14.42$).

The results are depicted on Fig. 17-8.3

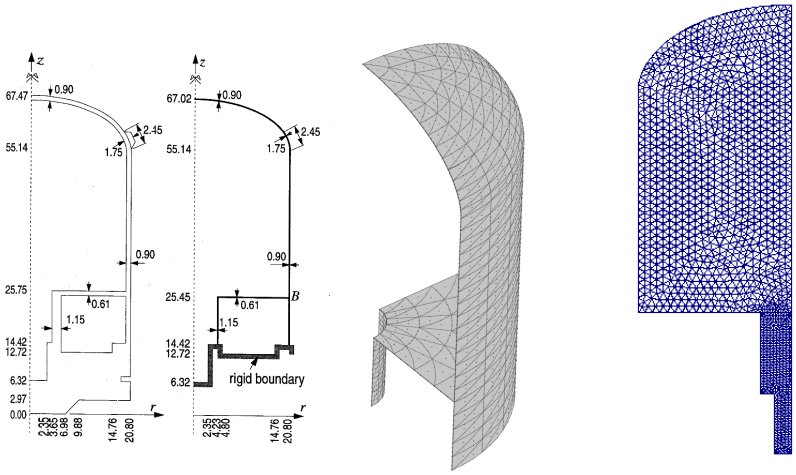

(a) Geometry adapted form Casadei and Halleux (1995) (b) Shell and fluid meshes

Figure 16: Reactor containment

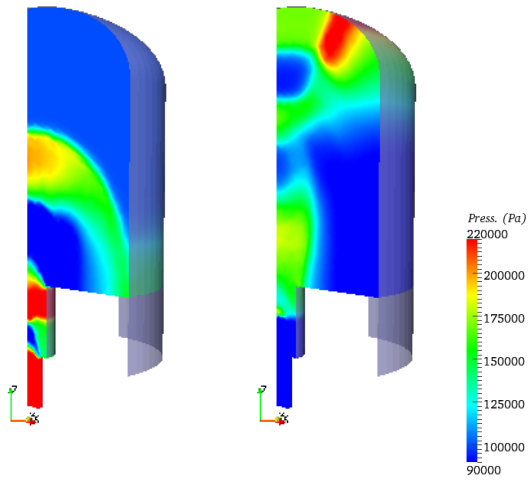

(a) t=0.05 s (b) t=0.11 s

Figure 17: Pressure distribution

9 CONCLUSION

A partitioned 3D computational code for non linear geometrical transient fluid-shell interaction analysis using the Finite Element Method is presented. Among the necessary components of the overall computational framework, are the shell and the fluid formulation. The shell formulation is able to deal with geometrical nonlinear dynamics of shells, using a methodology based on the minimum potential energy theorem written regarding nodal positions and generalized unconstrained vectors, not displacements and rotations, avoiding the use of large rotation approximations and its time integration is based on the Newmark method. The fluid solver is based on the arbitrary Lagrangian-Eulerian (ALE) description of fluid mechanics in order to accept moving boundaries and coupling with Lagrangian shell elements. The flow is consid-

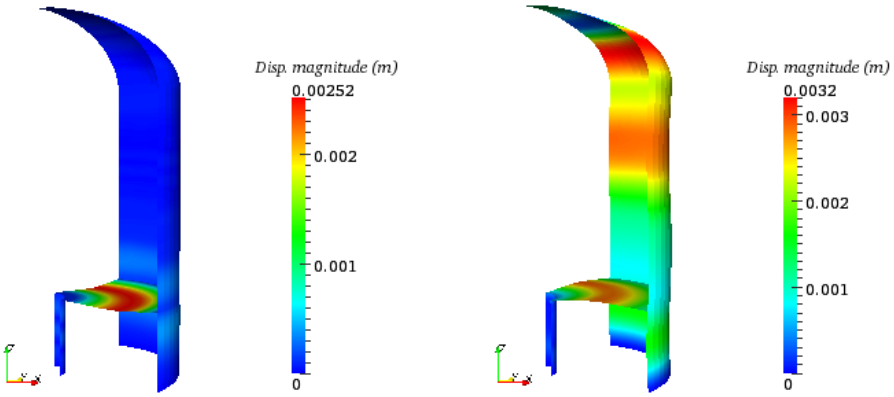

(a) t=0.05 s (b) t=0.11 s

Figure 18: Deformed structure

ered compressible and its time integration is explicit and based on characteristics, which introduces automatically stabilizing terms on stream direction. The coupling technique allow the use of non-matching nodes meshes for fluid and structure, which is done by mapping the fluid boundary nodes local positions over the shell elements and *vice versa*. Based on the presented examples we conclude that the proposed fluid solver, shell solver and coupling technique are completely adequate for fluid-structure simulations and should be deeply studied and extended also to incompressible flows.

REFERENCES

Bathe K.J. and Zhang H. Finite element developments for general fluid flows with structural interactions. *International Journal for Numerical Methods in Engineering*, 60:213–232, 2004.

Casadei F. and Halleux J.P. An algorithm for permanent fluid-structure interaction in explicit transient dynamics. *Computer Methods in Applied Mechanics and Engineering*, 128(3-4):231 – 289, 1995. ISSN 0045-7825.

Coda H.B. Two dimensional analysis of inflatable structures by the positional FEM. *Latin American Journal of Solids and Structures*, 6(3):187–212, 2009. ISSN 1679-7817.

Coda H.B. and Paccola R.R. Unconstrained Finite Element for Geometrical Nonlinear Dynamics of Shells. *Mathematical problems in engineering*, 2009. ISSN 1024-123X.

Coda H.B. and Paccola R.R. Improved finite element for 3d laminate frame analysis including warping for any cross-section. *Applied Mathematical Modelling*, 34(4):1107 – 1137, 2010. ISSN 0307-904X.

Donea J., Giuliani S., and Halleux J. An arbitrary lagrangian-eulerian finite element method for transient dynamic fluid-structure interactions. *Computer Methods in Applied Mechanics and Engineering*, 33(1-3):689 – 723, 1982. ISSN 0045-7825.

Fortuna O.A. *Técnicas computacionais para dinâmica dos fluidos*. EDUSP, São Paulo, Brasil, 2000.

Garelli L., Paz R.R., and Storti M.A. Fluid-structure interaction study of the start-up of a rocket engine nozzle. *Computers and Fluids*, 39(7):1208 – 1218, 2010. ISSN 0045-7930.

doi:DOI:10.1016/j.compfluid.2010.03.005.

Giordano J., Jourdan G., Burtschell Y., Medale M., Zeitoun D.E., and Houas L. Shock wave impacts on deforming panel, an application of fluid-structure interaction. *Shock Waves*, 14:103–110, 2005. ISSN 0938-1287.

Greco M. and Coda H.B. A simple and precise fem formulation for large deflection 2d frame analysis based on position description. *Computer Methods in Applied Mechanics and Engineering*, 193:3541–3557, 2004.

Maciel D.N. and Coda H.B. Positional description for non-linear 2d static and dynamic frame analysis by fem with reissner kinematics. In *Computational fluid and Solid Mechanics*. MIT, MIT, Boston, 2005.

Ogden R. Non-linear elastic deformations. *Engineering Analysis*, 1(2):119 – 119, 1984. ISSN 0264-682X.

Rifai S.M., Johan Z., Wang W.P., Grisval J.P., Hughes T.J., and Ferencz R.M. Multiphysics simulation of flow-induced vibrations and aeroelasticity on parallel computing platforms. *Computer Methods in Applied Mechanics and Engineering*, 174(3-4):393 – 417, 1999. ISSN 0045-7825.

Sanches R.A.K. and Coda H.B. Formulação bidimensional alternativa para a interação fluido-estrutura através do mef. In *XXIX Congresso Ibero Latino Americando de Métodos Computacionais em Engenharia - CILAMCE*. Maceió, Brazil, 2008a.

Sanches R.A.K. and Coda H.B. Simulação bidimensional de escoamentos compressíveis de fluido com contornos móveis através do mef. In *XXIX Congresso Ibero Latino Americando de Métodos Computacionais em Engenharia - CILAMCE*. Maceió, Brazil, 2008b.

Teixeira P.R.F. *Simulação Numérica da interação de escoamentos tridimensionais de fluidos compressíveis e incompressíveis e estruturas deformáveis usando o método de elementos finitos*. Doutorado em engenharia civil, Escola de Engenharia, Universidade Federal do Rio Grande do Sul, Porto Alegre, 2001.

Teixeira P.R.F.E. and Awruch A.M. Numerical Simulation of fluid-structure interaction using the finite element method. *Computers and Fluids*, 34:249–273, 2005.

Valiappan S. *Continuum mechanics fundamentals*. A. A. BALKEMA, Rotterdam, 1981.

Zienkiewicz O.C. and Taylor R.L. *The Finite Element Method, v2: Solid Mechanics*. Butterworth-heinemann Linacre house, 2000.